NANO LETTERS

Letter

pubs.acs.org/NanoLett

Wide Field Super-Resolution Surface Imaging through Plasmonic Structured Illumination Microscopy

Feifei Wei,[†] Dylan Lu,[†] Hao Shen,[†] Weiwei Wan,[†] Joseph Louis Ponsetto,[†] Eric Huang,[†] and Zhaowei Liu*[,†,‡]

[†]Department of Electrical and Computer Engineering and [‡]Materials Science and Engineering Program, University of California, San Diego, 9500 Gilman Drive, La Jolla, California 92093-0407, United States

Supporting Information

ABSTRACT: We experimentally demonstrate a wide field surface plasmon (SP) assisted super-resolution imaging technique, plasmonic structured illumination microscopy (PSIM), by combining tunable SP interference (SPI) with structured illumination microscopy (SIM). By replacing the laser interference fringes in conventional SIM with SPI patterns, PSIM exhibits greatly enhanced resolving power thanks to the unique properties of SP waves. This PSIM technique is a wide field, surface super-resolution imaging technique with potential applications in the field of high-speed biomedical imaging.

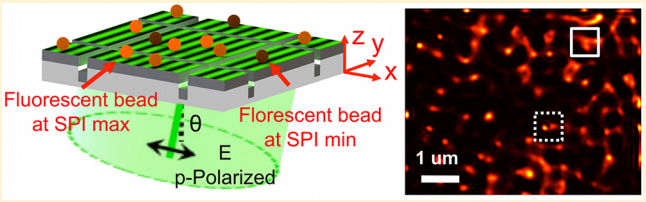

KEYWORDS: *Plasmonics, surface plasmon interference, structured illumination microscopy, super-resolution microscopy*

The optical microscope is an irreplaceable tool for biological research because light can probe biospecimens noninvasively. Despite its wide application in biology, the resolution of optical microscopy is fundamentally limited by diffraction, which means that objects with separations smaller than the diffraction limit cannot be resolved. In the visible spectrum, this minimum separation is on the order of several hundred nanometers, given by the Abbe limit $\lambda/(2NA)$, in which λ is the wavelength of the light and NA is the numerical aperture of the objective. Recently, biological research increasingly requires super-resolution microscopy methods for studying the structure and the dynamics of subcellular components. To achieve subdiffraction limited resolution, many novel imaging techniques have been proposed and experimentally demonstrated, such as near-field scanning optical microscopy (NSOM),[1−3] the far-field superlens (FSL),[4−6] hyperlens,[7−9] metalens,[10−13] stimulated emission depletion microscopy (STED),[14−16] single-molecule localization microscopy,[17−19] structured illumination microscopy (SIM),[20,21] and saturated structured illumination microscopy (SSIM),[22,23] super-resolution microscopy with high refractive index dielectric,[24−26] and so forth. Despite the tremendous successes of the aforementioned methods, each of these approaches has their own practical limitations.

Among the techniques mentioned above, SIM is uniquely suitable for high-speed biological imaging applications due to its wide field super-resolution imaging ability. Video-rate SIM has been used to reveal the tubulin and kinesin dynamics in living *Drosophila melanogaster* S2 cells.[27] SIM utilizes illumination with sinusoidally varying intensity to couple the high spatial frequency information of the object (Figure 1a, blue circles) to low spatial frequency information within the pass band of a microscope objective (Figure 1a, gray circle). Based on the far-field images acquired under multiple laterally translated sinusoidal illuminations, a subdiffraction limited image can be reconstructed. The resolution improvement of SIM relies on the spatial frequency of the illumination patterns, which is also limited by the numerical aperture of the objective. Thus, SIM normally achieves about 2-fold resolution improvement compared with conventional fluorescence microscopy, as is shown by the ratio of the radius of the SIM detectable region (large dashed circle) and the conventional microscopy detectable region (small gray circle) in Fourier space (Figure 1a). Further resolution improvement is possible by exploiting the nonlinear response of fluorescent dye using high power illumination in SSIM, but it results in increased phototoxicity and lower frame rate compared to SIM.[23]

To achieve higher resolution improvement without utilizing the nonlinear response of fluorophores, an illumination pattern with a period smaller than the diffraction limit is needed. The smaller the illumination period is, the higher the accessible spatial frequency information is, and thus a higher resolution image can be achieved. The surface plasmon (SP) is a good candidate to form subdiffraction limited interference patterns due to its large wave vector compared to light at the same frequency, as indicated by Figure 1c. Because of this unique property, SP is widely used in nanophotonic subwavelength scale applications.[4−9,28−39] By replacing laser interference patterns with SP interference (SPI) patterns with features smaller than $\lambda/(2NA)$, plasmonic structured illumination

Received: May 6, 2014
Revised: June 18, 2014
Published: July 11, 2014

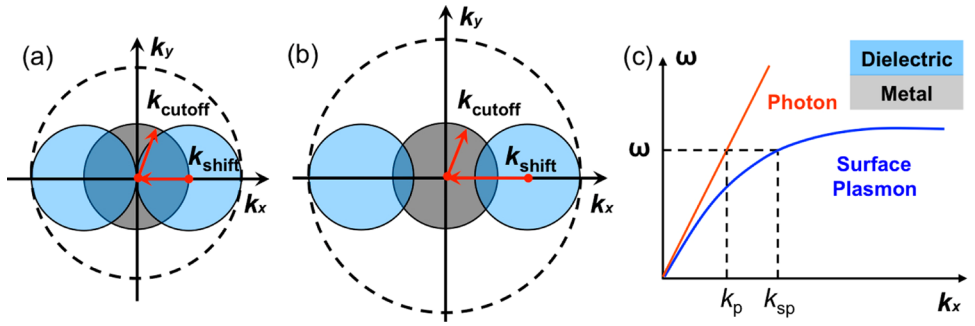

Figure 1. Illustration of the SIM and PSIM principles. (a–b) Resolution improvement representation in Fourier space. (a) SIM and (b) PSIM. The gray circles correspond to the spatial information within the pass band of conventional microscopy with k_{cutoff} representing its cutoff wave vector. The blue circles represent the sideband high spatial frequency information components accessible by SIM and PSIM, respectively, with k_{shift} representing the shift introduced by the illumination. The dashed circles represent the Fourier space region detectable by SIM and PSIM, respectively. (c) Schematic of the dispersion curves of the propagating photon in dielectric media (red line with k_p representing its wave vector) and the SP at the metal/dielectric interfaces (blue line with k_{sp} representing its wave vector).

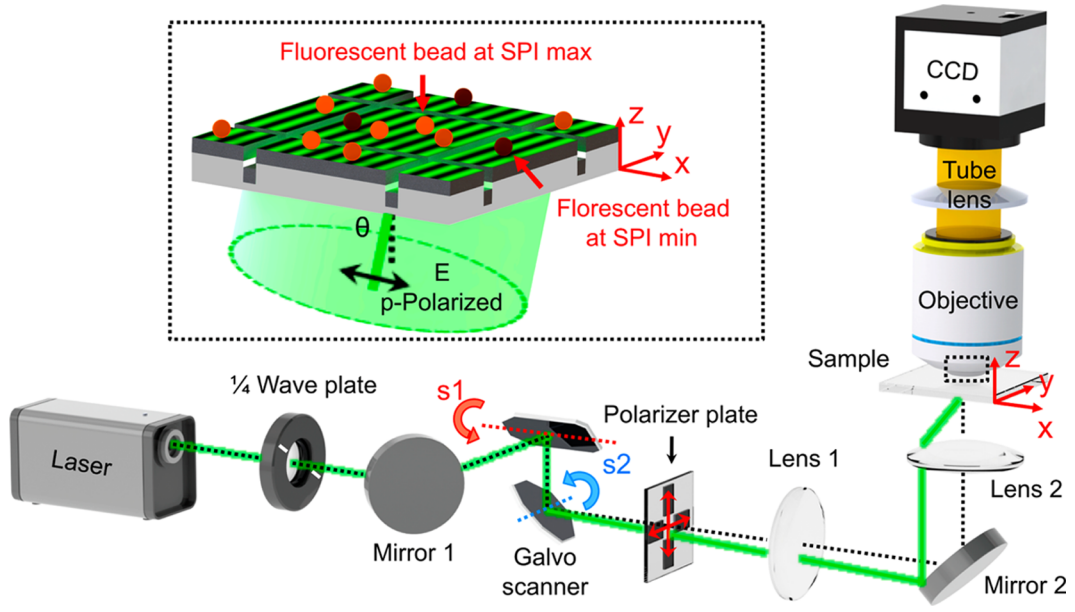

Figure 2. Schematics of the PSIM system. The illumination angle tuning in x–z and y–z planes are controlled by the rotation of the s2 and s1 mirror of the Galvo scanner, respectively, with the s2 mirror placed at the focal plane of lens 1 and the sample placed at the focal plane of lens 2. The polarization directions of the horizontal and vertical polarizer pairs (the gray rectangle regions) on the polarizer plate are indicated by the red arrows. Inset: a magnified view of the sample region.

microscopy (PSIM) possesses superior resolving power compared to conventional SIM, as shown in Figure 1b. In this paper, we present an experimental demonstration of this super-resolution PSIM technique.

The PSIM imaging system was built based on a Zeiss Axioskop microscope. The illumination module of the system consists of a laser light source, a two-dimensional (2D) Galvo scanner, and lens 1 and lens 2, as shown in the bottom part of Figure 2. When a plasmonic structure patterned with a 2D slit array is illuminated by the laser beam (Figure 2, inset), a SPI pattern is formed by the interference of the counter propagating SP waves generated at the adjacent slits. The lateral shift of the SPI pattern is realized by changing the illumination angle through the 2D Galvo scanner combined with lenses 1 and 2. The Galvo scanner is chosen due to its high-speed kHz rate angle tuning capability. The orientation of the SPI pattern is controlled by both the orientation of the slits as well as the polarization direction of the incident light. To excite a SP wave with the desired propagation direction and form a 1D SPI, a p-polarized light (with its polarization direction in the illumination plane) is needed. Finally, the fluorescence light excited by SPI illumination is collected by an objective and forms a diffraction-limited image through a tube lens onto an electron multiplying charge-coupled device (EMCCD), shown in the top part of Figure 2 (see Methods for the PSIM system details).

To demonstrate the PSIM concept, a slit array patterned plasmonic structure (Figure 3a–d) was designed and fabricated (see Methods for the fabrication details). Silver (Ag) was chosen because the SP at an Ag/dielectric interface can be generated for the entire visible spectrum with relatively low loss. To block direct transmission, a relatively thick Ag film (250 nm) was used in our design. The period and width of the slit array fabricated on the Ag film are 7.6 μm and 100 nm, respectively (Figure 3c, d). When light hits on the sample, SP waves are generated from the slits, and interference patterns are formed in between. The period of the slit array is on the order

dx.doi.org/10.1021/nl501695c | Nano Lett. 2014, 14, 4634–4639

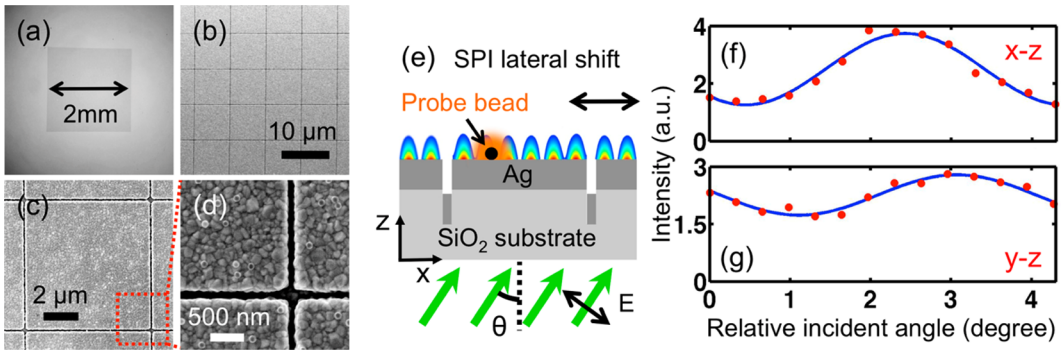

Figure 3. Sample fabrication and characterization. (a) Optical image of a large PSIM substrate. The total PSIM substrate area is 2 mm × 2 mm. (b–d) Scanning electron microscope (SEM) images of a PSIM substrate, showing an array of the patterned slits (b) one unit cell (c) and a further magnified view of the slits (d). (e) Schematic illustration of the SPI tuning scheme. As the incident angle θ changes, the SPI pattern shifts laterally (direction indicated by the horizontal black arrow). (f, g) Fluorescence intensity vs the relative incident angle in x–z (f) and y–z (g) plane, respectively. The measured data and the sinusoidal fit are represented by red dots and the solid blue lines, respectively.

of the SP propagation length, in order to achieve a relatively uniform SPI along its propagation direction.

To characterize the lateral translation of the SPI, fluorescent beads with a diameter of 100 nm were chosen as the SP field probes and placed on top of the patterned Ag film, as shown in Figure 3e (see Methods for the sample preparation and measurement details). The red dots in Figure 3f and g represent the fluorescence intensity variation of a single fluorescence bead with respect to the relative illumination angle in x–z and y–z plane (see the Supporting Information for illumination angle characterization), with the SPI pattern orientation along x and y directions, respectively. The fluorescence intensity curves are fitted to a sinusoidal function indicated by the solid blue lines, which confirms that the SPI is indeed generated and laterally translated as expected.

The super-resolved image was reconstructed from a total of six diffraction-limited subimages under 1D SPI illumination that was laterally translated along both x and y directions (see Methods for the measurement details). An iterative code, adapted from a blind structured illumination microscopy (Blind-SIM) reconstruction algorithm,[40] is used for image reconstruction (see the Supporting Information for algorithm details). Compared with the conventional fluorescence image (Figure 4a), the super-resolution image of three 100 nm diameter beads (Figure 4b) shows dramatic resolution improvement, confirmed by the SEM image in Figure 4c. The comparison of their corresponding Fourier transforms (shown in Figure 4d and e respectively) further proves that high spatial frequency information beyond the pass band of conventional fluorescence microscopy is indeed extracted from the six diffraction-limited images. The full-width at half-maximum (FWHM) (Figure 4f) of a single 100 nm diameter fluorescent bead decreases from 327 to 123 nm (averaged based on the red and green curves shown in Figure 4f), yielding a ~2.6-fold resolution improvement. This agrees with the theoretical enhancement factor, estimated based on the SP wave vector (k_{sp} = 1.44k_0, in which k_0 is the free space wave vector of the illumination laser) and the numerical aperture of the detection objective (NA = 1.0).

Figure 5 a–c shows the comparison of the conventional fluorescence image, its deconvolution, and the reconstructed super-resolution image over a large area. Because of the iterative recovery algorithm, the deconvolved image shows good resolution improvement for the isolated beads,[40] but the closely located beads still remain unresolved (Figure 5b, e, i).

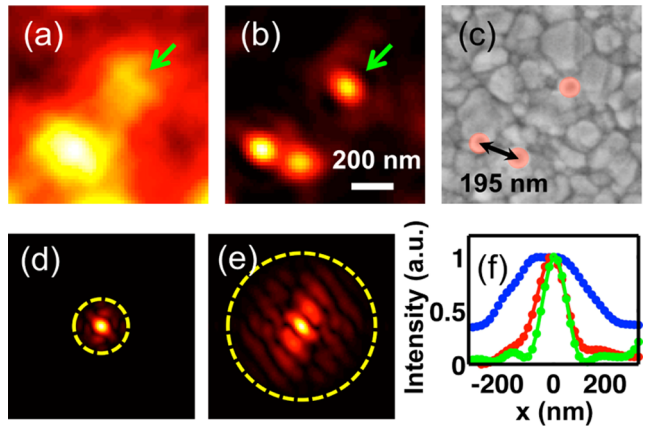

Figure 4. Demonstration of PSIM resolution improvement with a single bead. Fluorescence beads with 100 nm diameters were used as the object. (a) Conventional fluorescence image. (b) Reconstructed PSIM image. (c) The corresponding SEM image, with beads highlighted in pseudo color (red). (d–e) Fourier transform of (a–b), respectively. The color scale for a–b and d–e are the same, with range from 0 to 1. The yellow dashed circles in (d) and (e) indicate the optical transfer function (OTF) of the conventional microscope system and that of the PSIM system. (f) Fluorescence intensity cross-section comparison of the single bead indicated by the green arrows in a–b. The red, green, and blue lines correspond to the fluorescence intensity cross-section of the reconstructed PSIM image along two perpendicular directions and that of the conventional fluorescence image, respectively.

Two sets of beads, with center-to-center distance below the Abbe limit of conventional fluorescence microscopy ~290 nm and the Abbe limit of the conventional SIM microscopy ~140 nm, are resolved in the PSIM super-resolution image in Figure 5f and j, with bead center-to-center distance characterized by the SEM images in Figure 5g and k, respectively. The corresponding PSIM image intensity curves (the red curves in Figure 5l–m) clearly show two peaks, while the conventional fluorescence image and deconvolution image intensity curves (the blue and green curves in Figure 5l–m) only show one peak.

Compared with conventional fluorescence microscopy, PSIM achieves a ~2.6-fold resolution improvement due to the small period of the SPI illumination. The resolution of PSIM is given by $\lambda_{em}/(2NA + 2NA_{eff})$, in which NA_{eff} is defined as k_{sp}/k_{em} with k_{sp} and k_{em} representing the wave vector of the SP and

dx.doi.org/10.1021/nl501695c | Nano Lett. 2014, 14, 4634–4639

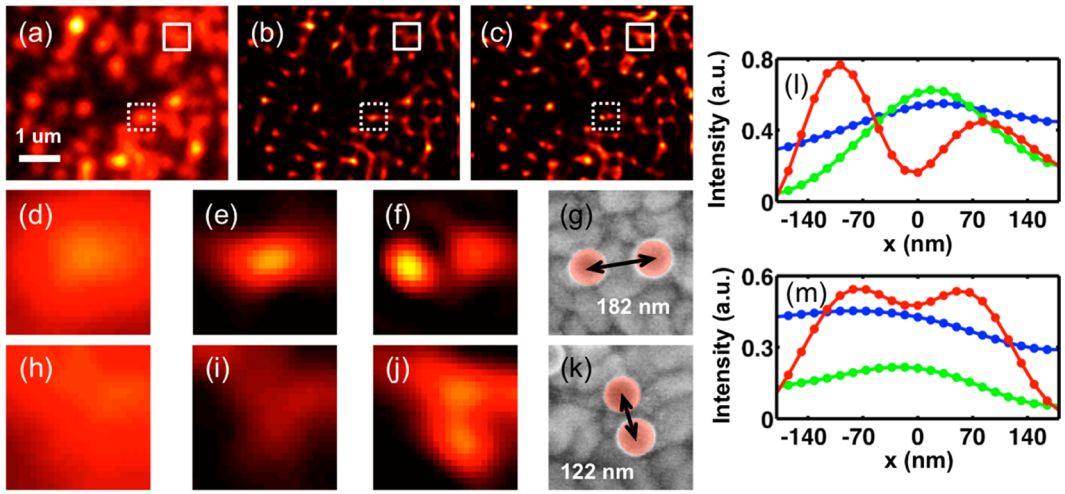

Figure 5. Demonstration of PSIM resolution improvement with closely located beads. (a) Conventional fluorescence image. (b) The corresponding deconvolution. (c) The reconstructed PSIM image. (d–f) Magnified images of the region within the white dashed boxes in a–c, respectively. (h–j) Magnified images within the white solid line boxes in (a–c), respectively. Fluorescence beads with 100 nm diameters were used as the object. The color scale for (a–f) and (h–j) are the same, with range from 0 to 1. (g, k) The corresponding SEM images with beads highlighted in pseudo color (red). (l–m) The corresponding fluorescence intensity cross-section comparison. The blue, green, and red lines correspond to the fluorescence cross-section of the conventional fluorescence images, the corresponding deconvolved images, and the PSIM reconstructed images, respectively.

emission light, respectively. With proper design, such as utilizing metal/dielectric multilayer geometries,[6,41] a very high k_{sp} could be engineered, leading to exceptionally large NA_{eff}. Therefore, the high resolution of the PSIM is predominantly determined by NA_{eff}. Experimentally, the resolution of the iteratively reconstructed super-resolution image also depends on the number of detected photons from the chromophores and moderately degrades as the number of photons decreases.[40]

Besides its super lateral resolution imaging capability, PSIM also provides high signal-to-noise ratio (SNR) by restricting the excitation of the fluorescence to a thin region very close to the metal/dielectric interface due to the evanescent nature of the SPs. The thickness of this thin region is determined by the z intensity decay length of the SPI field, which varies from several tens of nanometers to several hundreds of nanometers, depending on the wavelength used and the designed SP wave vector. For objects of interest that only exist very close to the interface, such as cell membranes, PSIM is a good tool to provide subdiffraction limited lateral resolution and eliminate the unwanted fluorescence signal from the dyes that are far away from the surface.

Compared with SP assisted scanning microscopy,[35] in which propagating SPs are focused to a subdiffraction limit region and scanned across the sample, the demonstrated PSIM is a wide field imaging technique. To reconstruct a super-resolution image, the excited 1D SPI only needs to be laterally translated three times for each direction. Moreover, the slit array configuration for SP excitation removes the imaging area constraint enforced by the SP decay length and extends the usable area to the whole patterned region. Since the SPI lateral translation is accomplished by tuning the incident angle, it is relatively easy to achieve high speed, e.g., with the Galvo scanning mirrors.[42] Due to its wide field imaging ability and the high-speed illumination angle tuning capability, the demonstrated PSIM technique has the potential to achieve video rate and be applied for super-resolution biospecimen dynamics studies, including single molecule level[27] based on the existing light sources and detection technologies. Moreover, a thin dielectric layer (10–20 nm) could be added on top of the metal film, serving as a protection layer to separate the biospecimens and the metal, as well as a spacer layer to reduce the quenching of the fluorescent dyes.[43,44]

In conclusion, we have presented a proof-of-concept experimental demonstration of the wide-field PSIM technique. Utilizing slit-coupled SPI as the illumination, PSIM is capable of achieving higher resolution than conventional SIM. Although the reconstructed PSIM images show 2.6-fold resolution improvement in the present experiment, the ultimate PSIM resolution is only limited by the achievable wave vectors of the SPs and could be drastically improved by plasmonic mode engineering in more optimized structures. The new PSIM may lead to important applications where a high-speed super-resolution imaging tool is needed.

Methods. *PSIM Substrate Fabrication.* A fused silica (SiO_2) wafer was chosen as the substrate due to its transparency in the visible spectrum. The designed slit array pattern was produced on the fused silica substrate using nanolithography. The patterned resist served as a dry etching mask for transferring the pattern into the fused silica, followed by the standard piranha solution cleaning process to remove the resist residue. Finally, a 4 nm adhesion layer and a 250 nm Ag film were deposited on the patterned substrate using electron beam deposition at $2e^{-7}$ Torr.

PSIM Sample Preparation. In our experiments, 100 nm diameter fluorescent beads (Life Technologies, F8800) were used as the probes for SPI shift characterization and the object for PSIM imaging capability demonstration. A sample of 1 μL of the fluorescent bead solution was drop-casted onto the slit-array patterned plasmonic structure and dried in air, with the sparsity of the beads controllable by the solution concentration (about 1.2×10^{10} beads/mL for experiments shown in Figures 3–5).

PSIM Measurements. The PSIM measurements were performed on a custom-built PSIM platform shown in Figure 2. The linearly polarized light coming out of a 200 mW 532 nm laser is converted to circularly polarized light by a 1/4 waveplate and then reflected to the 2D Galvo scanner (Cambridge Technology 6210H) and the lens system. These

dx.doi.org/10.1021/nl501695c | Nano Lett. 2014, 14, 4634–4639

elements control the illumination angle variation in $x-z$ and $y-z$ planes. After passing the polarizer plate placed between the scanner and the lens system, only illumination light with proper polarization is allowed to illuminate the PSIM substrate for exciting the desired 1D SPI pattern. As the incident angle θ varies in $x-z$ and $y-z$ plane, the phase difference (ϕ) between the SP waves excited at the two adjacent edges changes accordingly based on $\phi = 2\pi \cdot d \cdot \sin(\theta)/\lambda$, in which d is the period of the slit array and λ is the wavelength of the laser, and results the lateral translation of the SPI pattern. The PSIM fluorescent images formed by SPI illumination were then collected by a 63× water dipping objective (Zeiss W Plan-Apochromat 63x/1.0 Ph3) and recorded by an EMCCD (Andor 897) with 0.15 s exposure, with a 593 ± 20 nm band-pass filter placed in the detection light path. To compensate the angle-dependent illumination intensity variation, the detected fluorescent images were normalized by the corresponding intensity of the scattered laser light at the slits under the same illumination angle. The illumination and image acquisition modules were synchronized by a Labview-controlled data acquisition card (DAQ).

For demonstrating the lateral translation of the SPI pattern, 14 diffraction-limited images were recorded, with the relative illumination angle varying from 0° to about 4.3° with equal steps in either the $x-z$ or $y-z$ plane. To reconstruct a super-resolution image, only three diffraction-limited images, illuminated by three 1D SPI patterns with about 1/3 of the interference period lateral shift between each other, are needed for each direction. To generate this 1/3 period SPI lateral shift, the phase difference between the SP waves excited at the adjacent slits (ϕ) changes by $2\pi/3$ each time. This process was performed for both x- and y-oriented interference patterns to achieve two-dimensional resolution improvement, yielding a total of six image acquisitions. The conventional fluorescence images were collected using the same objective and EMCCD under light emission diode (LED) illumination, but with a 523 ± 10 nm and a 585 ± 10 nm filter as the illumination and detection filter, respectively.

■ ASSOCIATED CONTENT

Ⓢ Supporting Information

Additional details on the illumination angle characterization, image reconstruction, and deconvolution algorithm. This material is available free of charge via the Internet at http://pubs.acs.org.

■ AUTHOR INFORMATION

Corresponding Author

*E-mail: zhaowei@ece.ucsd.edu.

Notes

The authors declare no competing financial interest.

■ ACKNOWLEDGMENTS

This work was supported by the Gordon and Betty Moore Foundation and the National Science Foundation (NSF) Electrical, Communications and Cyber Systems (ECCS; grant no. 0969405). The authors thank Carl Zeiss for providing the loaned microscope and thank L. Wang for useful discussions on numerical reconstruction algorithms.

■ REFERENCES

(1) Ash, E. A.; Nicholls, G. *Nature* **1972**, *237*, 510−512.
(2) Lewis, A.; Isaacson, M.; Harootunian, A.; Muray, A. *Ultramicroscopy* **1984**, *13*, 227−231.
(3) Pohl, D. W.; Denk, W.; Lanz, M. *Appl. Phys. Lett.* **1984**, *44*, 651−653.
(4) Durant, S.; Liu, Z.; Steele, J. M.; Zhang, X. *J. Opt. Soc. Am. B* **2006**, *23*, 2383−2392.
(5) Liu, Z.; Durant, S.; Lee, H.; Pikus, Y.; Fang, N.; Xiong, Y.; Sun, C.; Zhang, X. *Nano Lett.* **2007**, *7*, 403−408.
(6) Xiong, Y.; Liu, Z.; Sun, C.; Zhang, X. *Nano Lett.* **2007**, *7*, 3360−3365.
(7) Jacob, Z.; Alekseyev, L. V.; Narimanov, E. *Opt. Express* **2006**, *14*, 8247−8256.
(8) Liu, Z.; Lee, H.; Xiong, Y.; Sun, C.; Zhang, X. *Science* **2007**, *315*, 1686.
(9) Rho, J.; Ye, Z.; Xiong, Y.; Yin, X.; Liu, Z.; Choi, H.; Bartal, G.; Zhang, X. *Nat. Commun.* **2010**, *1*, 143.
(10) Lerosey, G.; de Rosny, J.; Tourin, A.; Fink, M. *Science* **2007**, *315*, 1120−1122.
(11) Lemoult, F.; Lerosey, G.; de Rosny, J.; Fink, M. *Phys. Rev. Lett.* **2010**, *104*, 203901.
(12) Lemoult, F.; Fink, M.; Lerosey, G. *Nat. Commun.* **2012**, *3*, 889.
(13) Lu, D.; Liu, Z. *Nat. Commun.* **2012**, *3*, 1205.
(14) Hell, S. W.; Wichmann, J. *Opt. Lett.* **1994**, *19*, 780−782.
(15) Klar, T. A.; Jakobs, S.; Dyba, M.; Egner, A.; Hell, S. W. *Proc. Natl. Acad. Sci. U.S.A.* **2000**, *97*, 8206−8210.
(16) Westphal, V.; Rizzoli, S. O.; Lauterbach, M. A.; Kamin, D.; Jahn, R.; Hell, S. W. *Science* **2008**, *320*, 246−249.
(17) Rust, M. J.; Bates, M.; Zhuang, X. *Nat. Methods* **2006**, *3*, 793−796.
(18) Huang, B.; Wang, W.; Bates, M.; Zhuang, X. *Science* **2008**, *319*, 810−813.
(19) Betzig, E.; Patterson, G. H.; Sougrat, R.; Lindwasser, O. W.; Olenych, S.; Bonifacino, J. S.; Davidson, M. W.; Lippincott-Schwartz, J.; Hess, H. F. *Science* **2006**, *313*, 1642−1645.
(20) Heintzmann, R.; Cremer, C. *Proc. SPIE* **1998**, *3568*, 185−196.
(21) Gustafsson, M. G. L. *J. Microsc.* **2000**, *198*, 82−87.
(22) Heintzmann, R.; Jovin, T. M.; Cremer, C. *J. Opt. Soc. Am. A* **2002**, *19*, 1599−1609.
(23) Gustafsson, M. G. L. *Proc. Natl. Acad. Sci. U.S.A.* **2005**, *102*, 13081−13086.
(24) Frohn, J. T.; Knapp, H. F.; Stemmer, A. *Proc. Natl. Acad. Sci. U.S.A.* **2000**, *97*, 7232−7236.
(25) Sentenac, A.; Belkebir, K.; Giovannini, H.; Chaumet, P. C. *J. Opt. Soc. Am. A* **2009**, *26*, 2550−2557.
(26) Girard, J.; Scherrer, G.; Cattoni, A.; Le Moal, E.; Talneau, A.; Cluzel, B.; de Fornel, F.; Sentenac, A. *Phys. Rev. Lett.* **2012**, *109*, 187404.
(27) Kner, P.; Chhun, B. B.; Griffis, E. R.; Winoto, L.; Gustafsson, M. G. L. *Nat. Methods* **2009**, *6*, 339−342.
(28) Liu, Z.; Steele, J. M.; Lee, H.; Zhang, X. *Appl. Phys. Lett.* **2006**, *88*, 171108.
(29) Bartal, G.; Lerosey, G.; Zhang, X. *Phys. Rev. B* **2009**, *79*, 201103.
(30) Sentenac, A.; Chaumet, P. C.; Belkebir, K. *Phys. Rev. Lett.* **2006**, *97*, 243901.
(31) Chung, E.; Kim, Y. H.; Tang, W. T.; Sheppard, C. J. R.; So, P. T. C. *Opt. Lett.* **2009**, *34*, 2366−2368.
(32) Wei, F.; Liu, Z. *Nano Lett.* **2010**, *10*, 2531−2536.
(33) Wang, Q.; Bu, J.; Tan, P. S.; Yuan, G. H.; Teng, J. H.; Wang, H.; Yuan, X. C. *Plasmonics* **2012**, *7*, 427−433.
(34) Gjonaj, B.; Aulbach, J.; Johnson, P. M.; Mosk, A. P.; Kuipers, L.; Lagendijk, A. *Nat. Photonics* **2011**, *5*, 360−363.
(35) Gjonaj, B.; Aulbach, J.; Johnson, P. M.; Mosk, A. P.; Kuipers, L.; Lagendijk, A. *Phys. Rev. Lett.* **2013**, *110*, 266804.
(36) Luo, X.; Ishihara, T. *Appl. Phys. Lett.* **2004**, *84*, 4780−4782.
(37) Liu, Z.; Wei, Q. H.; Zhang, X. *Nano Lett.* **2005**, *5*, 957−961.
(38) Shao, D. B.; Chen, S. C. *Nano Lett.* **2006**, *6*, 2279−2283.
(39) Pan, L.; Park, Y.; Xiong, Y.; Ulin-Avila, E.; Wang, Y.; Zeng, L.; Xiong, S.; Rho, J.; Sun, C.; Bogy, D. B.; Zhang, X. *Sci. Rep.* **2011**, *1*, 175.

(40) Mudry, E.; Belkebir, K.; Girard, J.; Savatier, J.; Le Moal, E.; Nicoletti, C.; Allain, M.; Sentenac, A. *Nat. Photonics* **2012**, *6*, 312−315.
(41) Xiong, Y.; Liu, Z.; Zhang, X. *Appl. Phys. Lett.* **2008**, *93*, 111116.
(42) Wilt, B. A.; Burns, L. D.; Ho, E. T. W.; Ghosh, K. K.; Mukamel, E. A.; Schnitzer, M. J. *Annu. Rev. Neurosci.* **2009**, *32*, 435−506.
(43) Weber, W. H.; Eagen, C. F. *Opt. Lett.* **1979**, *4*, 236−238.
(44) Barnes, W. L. *J. Mod. Opt.* **1998**, *45*, 661−699.

dx.doi.org/10.1021/nl501695c | *Nano Lett.* 2014, 14, 4634−4639